A Rate-Difference Disturbance Observer Control for a Timing-Belt Servo System

Zhiyong Yu, Tao Yang, Yong Ruan, Tianrong Xu, and Tao Tang, *Member, IEEE*

***Abstract*—The belt-drive control enables the mechanical system to gain the advantages of lightweight, vibration absorption, and high torque, while it brings strong nonlinear disturbances due to friction, backlash, and flexibility. Therefore an improved disturbance observer (DOB) control method based on the dual-rate loop structure is proposed in this article to suppress these disturbances. Only a linear low-frequency device model is required, which indicates that this method avoids the dependence on accurate identification of the nonlinear uncertain systems. The rate information on the motor-side is replaced with the input signal of inner loop due to the high bandwidth of inner motor loop, which greatly simplifies the design of the control system. In the case of insufficient system bandwidth, the proposed method integrates the favorable information of the load-side and the motor-side under the DOB framework. And the speed-commutation spikes and chatters resulting from disturbances on the flexible transmission chain can be more effectively suppressed by the proposed control structure compared with the conventional methods.**

***Index Terms*—Belt-drive, disturbance observer (DOB), low-bandwidth control, Q-filter, spike suppression.**

I. Introduction

WHILE the mechanical servo systems move toward high-speed and high-precision, increased precision components will bring the problems of large size, heavy load, and excessive power-consumption, for which many researchers tend to employ nondirect drive in modern servo systems to get a lightweight structure. In recent decades, the synchronous belt drive, or namely the timing-belt drive, has emerged as a novel type of transmission mode, which is worth further exploring. As an important nondirect drive mode, it shows advantages of weight reduction, vibration absorption, long-span, low-power, high-torque, and compact layout, as well as the characteristics of low-cost, convenient installation, low mechanical noise, and wide range of speed regulation [1]. Moreover, combined with the benefits of gear-drive, chain-drive, and belt-drive, it meshes with the groove of the pulley using its tooth-shaped working surface [2]. It can be applied to various mechanical movements including those in automobiles, textiles, agricultural machinery, printing, and robot motion.

However, due to the low structural stiffness of the timing-belt drive system, difficulties in control strategy will inevitably arise. Under the action of an external load, the strong elastic deformation will contribute to the high-order mode and uncertain dynamics of the system, which will make the system exhibit resonance, viscosity, hysteresis, friction, backlash, coupling, and other nonlinear characteristics. When reciprocating motion or low-speed operation occurs, the closed-loop performance may deteriorate owing to the hysteresis and the dead-zone of the mechanical control system. Additionally, negatively affected by the nonperiodic change of tension force, the fatigue and wear of the timing-belt system will reduce the angular velocity between the pulleys. It is also necessary to implement a fault-tolerant control technology in the timing-belt systems when dealing with a challenging disturbance environment [3]. In order to solve the difficulties of the timing-belt system in tracking accuracy and stability performance, the current research works mainly focus on the disturbance suppression in the following three aspects:

First, the most direct and effective method to improve the performance is to increase the tension force by strengthening the stiffness of the timing-belt. Nevertheless, the composed material used for the timing-belt is susceptible to changes in temperature and humidity in the environment, resulting in the fluctuation of the stiffness coefficient. In addition, the multimotor drive, an improvement of the control bandwidth in the timing-belt mechanical system [4], poses an extra burden on the components and materials, as well as involves the problems associated with the synchronization and coordination of multimotor control system. For the most part, these mechanical modifications have a very limited effect on the performance improvement.

Second, model-based compensation control methods are also widely used in the field of flexible belt transmission to improve control performance [5], [6]. An accurate compensation model needs numerous nonlinear dynamics to be considered in the mathematical equations of the model. Whereas they face challenges in measuring or simply estimating some parameters

Manuscript received June 14, 2021; revised August 30, 2021; accepted October 14, 2021. Date of publication November 3, 2021; date of current version June 6, 2022. This work was supported in part by Sichuan Province Science and Technology Program. *(Corresponding author: Tao Tang.)*

Zhiyong Yu and Yong Ruan are with the Key Laboratory of Optical Engineering, Chinese Academy of Sciences, Chengdu 610209, China, and with the Institute of Optics and Electronics, Chinese Academy of Science, Chengdu 610209, China, and also with the University of Chinese Academy of Sciences, Beijing 100049, China (e-mail: zhiyong.yu662@gmail.com; ruanyong20@mails.ucas.ac.cn).

Tao Yang, Tianrong Xu, and Tao Tang are with the Key Laboratory of Optical Engineering, Chinese Academy of Sciences, Chengdu 610209, China, and also with the Institute of Optics and Electronics, Chinese Academy of Science, Chengdu 610209, China (e-mail: taoyang90@ioe.ac.cn; tianrongxu5802@ioe.ac.cn; taotang@ioe.ac.cn).

Color versions of one or more figures in this article are available at https://doi.org/10.1109/TIE.2021.3123642.

Digital Object Identifier 10.1109/TIE.2021.3123642

in nonlinear links, only rough or ideal substitute values under certain assumptions are given, greatly weakening the accuracy of compensation [6]. For example, only Coulomb friction and viscous friction models are considered in dynamic recognition, resulting in a relatively limited description of the friction process. Furthermore, there are also many difficulties in analyzing belt tension, traction force, centrifugal force, and contact area. Generally, there is a tradeoff between precision and simplicity of control model [7]. Relying on a reliable system model, the estimation of the resonance ratio significantly contributes to the success of the vibration control design [8]. In the current research, accurate system models adopt a more comprehensive model description [7] and real-time online parameter capture methods [9]. In particular, recursive least squares have been used in model estimation actively and widely, and the establishment of an adaptive mechanism [5] or a model prediction mechanism [10] can reinforce the nonlinear model of the system. The efforts made in the previous studies are usually well validated in simulations or linear guide-based belt transmission systems. For that complex belt transmission equipment with dynamic coupling and multidegree-of-freedom coupling effect, there will be marked interdependence between the closed-loop poles, which poses huge challenges to physical modeling, order identification, and parameter identification.

Third, it is particularly necessary to mention some widely and far-reaching control technologies in this field. Sliding mode control (SMC) has excellent disturbance rejection performance for nonlinear systems, and it has been applied in the timing-belt system [11]. In order to weaken the "chatter" generated by the switching of control law and raise the system response speed, a belt stretching estimator [12] or an asymptotic observer [8] is proposed to improve the SMC, leading to increase the complexity of control algorithm design. In addition, adaptive SMC [13], neuro SMC [14], fuzzy control [2], genetic algorithm [15], learning control [16], and boundary control [17] have also been utilized in the research of antidisturbance of the belt-drive servo system. The benefits of these incorporating model-based and data-driven control algorithms based on the nonlinear controller are obvious, while practice shows that they are susceptible to rule bases, training models, and constraint equations with some trial-and-error costs. To sum up, the complexity of algorithm structure and the resulting difficulty in design, analysis, and real-time computing require further attention in the coming research.

Finally, and most critically, the disturbance observer (DOB) control is an attractive method for the disturbances that cannot be directly measured, without using any additional sensors. DOB is a popular robust control tool due to its simplicity, flexibility, and efficacy [18], and it is also well applied in the control strategy of flexible transmission systems [8], [19]. Moreover, the disturbance observers can be utilized in conjunction with model predictive control [10], singular perturbation theory [20], nonsingular terminal SMC [21], and robust control [22] to achieve multistage composite control that reduces the impact of unmodeled characteristics at high frequency. For the nonlinear systems with multiple stochastic or deterministic disturbances, the DOB-based control method like elastic control [23] or H_∞ refined antidisturbance control [24] is very effective. Notably, these current DOB studies are particularly concentrated on the processing on the motor-side of the system, meaning that the disturbance suppression is only effective on the motor-side [25]. It has been verified because ideally, the performance of the load-side controller improves when the uncertainty on the motor-side is successfully compensated [26], [27]. However, in a practical belt-drive system, the uncertain dynamics on the motor-side are often amplified by the flexible coupling device. As the shaft torque can only be observed or adjusted through the speed or current information presented on the motor-side, the suppression effect is restricted. The current research also mentioned the use of dynamic DOB combined with backstepping control to solve the uncertainty on the load-side [25], and the DOB-based double-disturbance compensation has also played a positive effect in practice [28]. For a multi-inertia and highly motor-load coupled drive system like the flexible belt-drive system, it is necessary to find a pervasive and effective solution based on DOB on the load-side.

Based on the aforementioned research status, the implementation concept of the DOB will be discussed from the signal measurement perspective in this article; thus, the rate-difference information between the load-side and the motor-side has been introduced as a new DOB scheme. This control structure incorporating both rate information is implemented in a dual-rate stabilization loop. Overall, the contributions of this article are as follows.

1) The proposed control structure is not highly dependent on the high-precision model identification of the belt-drive system. The smooth execution of control structure requires no need to derive an extremely refined mathematical model but entail combination with frequency response test data.
2) The proposed method involves a linear controller. It fully incorporates favorable information between the motor-side and the load-side, and successfully narrows the errors made by comprehensive nonlinear disturbance without involving complex mathematical derivations and calculations.
3) The influence of filter bandwidth selection and modeling accuracy on system stability and performance in the DOB structure is argued, which provides direct guidance for the control structure design.

The rest of this article is organized as follows.

Section II presents the modeling of the belt-drive servo system, Section III deduces and analyzes the DOB control structure, Section IV provides the experimental verification. Section V concludes this article.

II. Modeling of Belt-Drive System

Understanding the system operation mechanism is the first step to establish the control system; therefore, we focus on a typical belt-drive system model analysis. The belt-drive system is roughly separated into electrical subsystem and mechanical subsystem in order to understand the proposed control structure well. It introduces the electromagnetic excitation model before

the motor-side speed output in the first part, and elaborates the mechanical transmission model between the motor-side speed output and the load-side speed output in the following part. A typical belt-drive system is built as shown in the following. It is composed of motor, gearbox reducer, driving pulley, driven pulley, timing-belt, and load. The output torque τ_0 at the end of the motor axis drives the driving pulley to rotate through the gearbox. Then, the driving pulley actuates the driven pulley and the load through the timing-belt for positioning movement.

A. Electrical Subsystem

The low-power brushless dc motor is chosen as the electrical drive supplier because of its advantages such as small size, convenient speed regulation, and low electromagnetic noise. The equilibrium equation of the conventional brushless dc motor can be derived based on its excitation principle as follows:

$$U_a = E + R_m I_m + L_m \dot{I}_m \tag{1}$$

$$E = K_e \dot{\theta}_m \tag{2}$$

$$\tau_m = K_m I_m \tag{3}$$

$$\tau_m = \tau_0 + \tau_q + C_m \dot{\theta}_m + J_m \ddot{\theta}_m \tag{4}$$

where U_a is the rated voltage of the motor, and E and K_e represent the average and the coefficient of back-EMF of armature, respectively. I_m, R_m, and L_m express the average current, average resistance, and average self-inductance of the armature windings, respectively. τ_m, τ_0, and τ_q denote the electromagnetic torque, the output torque, and the internal disturbance torque of the motor, respectively. K_m is the torque coefficient, and C_m and J_m indicate the damping coefficient and inertia moment of the motor, respectively. θ_m is the rotation angle of motor axis. The electrical subsystem can be considered to exhibit second-order system characteristics as follows if the disturbance torque and load are neglected:

$$G_m(s) = \frac{K_m}{L_m J_m s^2 + (L_m C_m + R_m J_m)s + (R_m C_m + K_e K_m)}. \tag{5}$$

B. Mechanical Subsystem

In the mechanical transmission part, the following are assumed.

(1) The motor can ensure high dynamic torque response with a negligible time-delay [8].

(2) The motor axes are rigidly connected with the gearbox driving wheel.

(3) The resistance torque of the gearbox and transmission link on the rod can be expressed by an uniform damping factor. The following mechanical equations can be established:

$$\tau_0 = J_{g1} \ddot{\theta}_m + J_{g2} \ddot{\theta}_a + J_a \ddot{\theta}_a + c_k \dot{\theta}_a + \tau_p + \tau_f \tag{6}$$

$$\tau_p = (J_p + J_z + J_b) \ddot{\theta}_p \tag{7}$$

$$\ddot{\theta}_p = K_a \ddot{\theta}_a \tag{8}$$

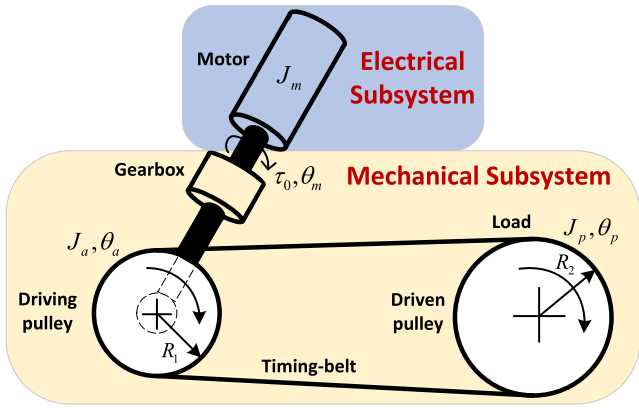

Fig. 1. Typical belt-drive system.

$$\theta_m = \theta_a z \tag{9}$$

where θ_m is the rotation angle of motor axis and the gearbox driving wheel [8], θ_a is the rotation angle of the gearbox driven wheel and the belt-driving pulley, and θ_p is the rotation angle of the belt-driven pulley. J_{g1} and J_{g2} are the inertia moment of the gearbox-driving wheel and the gearbox-driven wheel, respectively. J_a and J_p are corresponding the inertia moment of the belt-driving pulley and the belt-driven pulley, respectively. J_z and J_b indicate the inertia moment of the load and the belt, respectively. c_k represents the damping coefficient of the gearbox and transmission link on the rod. K_a shows the acceleration transfer coefficient of belt pulley and K_a^* is a coefficient related to K_a. τ_p and τ_f denote the acceleration torque of the load and the unknown friction torque or elastic torque, respectively. z is the transmission ratio of the gearbox. The following formula can be obtained after organizing the abovementioned equations:

$$\tau_0 = [z J_{g1} + J_{g2} + J_a + (J_p + J_z + J_b) K_a] \ddot{\theta}_a + c_k \dot{\theta}_a + \tau_f. \tag{10}$$

Let $h_k = [z J_{g1} + J_{g2} + J_a + (J_p + J_z + J_b) K_a]$. Thus, the mechanical subsystem can be considered to exhibit one-order system characteristics as follows if the disturbance torque is neglected:

$$G_p(s) = \frac{K_a^*}{c_k + h_k s}. \tag{11}$$

It is not accurate to regard the mechanical transmission part as a simple one-order system since the friction torque, elastic torque, disturbance inputs, and each transfer coefficients are unpredictable and nonlinear. It needs to be verified in conjunction with the frequency response tests later.

III. Research on Disturbance Suppression of Observer

A. Basic Design of Dual-Rate Loop

For the multi-inertia system with high-precision encoder on the load-side, the full closed-loop control mode is often used in engineering to obtain highly reliable control performance. As it was shown in Fig. 4, controllers C_m and C_v were used to control the electrical subsystem and mechanical subsystem respectively,

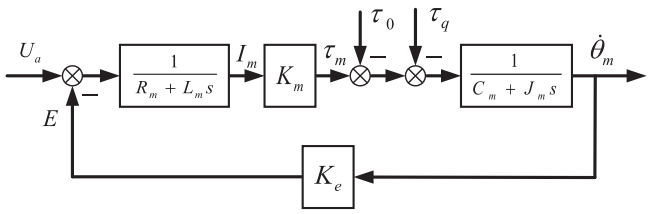

Fig. 2. Electrical subsystem transfer block diagram.

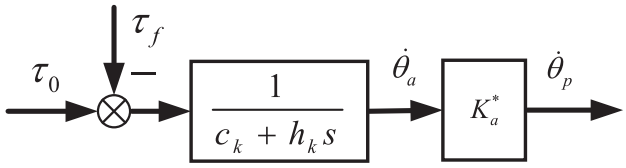

Fig. 3. Mechanical subsystem transfer block diagram.

which means a dual-rate loop structure based on full closed-loop was formed. ξ represents the measurement noise of the sensor. On the motor-side, a commercial driver is utilized to adjust the current and rate of the control object $G_m(s)$ with high precision to ensure the reliable linear control object $M(s)$. Assuming that C_m has completely suppressed the disturbance torque τ_q inside the motor, that is to say, the bandwidth of the motor is designed to be high enough. It can be assumed that $M(s)$ retains the same transfer order as $G_m(s)$. In addition, the transfer moment and elastic torsional moment are simplified by transfer coefficient K_r to obtain the linear control object $P(s)$ on the load-side. If uncertain unmodeled dynamics are considered, $P(s)$ can be assumed to obtain higher order dynamics than $G_p(s)$, which is detrimental for the control system. Based on the principle of simplification, the rough model $M(s)$ and $P(s)$ as follows are selected:

$$M(s) = \frac{1}{T_1^2 s^2 + 2T_1\xi_1 s + 1} \tag{12}$$

$$P(s) = \frac{T_1^2 s^2 + 2T_1\xi_1 s + 1}{T_2^2 s^2 + 2T_2\xi_2 s + 1} \tag{13}$$

B. Two-Degree-of-Freedom Control Structure

The disturbances made by the nonlinear characteristics of the system are complicated, especially in the low-speed and speed-commutation regions. To eliminate the disturbances, we choose to add a DOB to the dual-rate loop. The main idea of DOB is to estimate the disturbance by measuring the error between the actual system output and the nominal model output, then eliminate this estimated value by a feedforward signal. The effective rate-difference information in the dual-rate loop structure is combined with the observer principle in Fig. 5, where $C_v(s)$ is the speed controller to be designed. $Q(s)$ is a low-pass filter, which is used to ensure the causality of system and achieve the pass of disturbance estimation signal, and the cut-off of detection noise. P_n represents the inverse system of model $P(s)$. The rate-difference between the load-side and motor-side is accessed to implement the DOB, and the real-time feedforward compensation is carried out [29].

The rate closed-loop of motor makes its input and output nearly equal in fact; therefore, the speed output of the motor-side can be moved forward, which is shown in Fig. 6. Thus, the output $\dot{\theta}$ can be expressed with speed reference y_v, disturbance input d, and measurement noise ζ as follows:

$$\dot{\theta}_p = G_{y_v\dot{\theta}_p}(s)y_v + G_{d\dot{\theta}_p}(s)d + G_{\zeta\dot{\theta}_p}(s)\zeta \tag{14}$$

where

$$G_{y_v\dot{\theta}_p}(s) = \frac{C_v MPP_n}{P_n + C_v MPP_n + (P - P_n)Q} \tag{15}$$

$$G_{d\dot{\theta}_p}(s) = \frac{PP_n(1 - Q)}{P_n + C_v MPP_n + (P - P_n)Q} \tag{16}$$

$$G_{\zeta\dot{\theta}_p}(s) = \frac{C_v MPP_n + PQ}{P_n + C_v MPP_n + (P - P_n)Q} \tag{17}$$

where (16) represents the error transfer function from disturbance to output, and it can be concluded that $G_{d\dot{\theta}_p}(s) = 0$ when $Q(s) = 1$; therefore, the error is optimally suppressed. Equation (16) explains the reason why the proposed method in this article can perform error suppression. It is necessary to make the bandwidth of a low-pass filter wider, that is, the wider the frequency band of $Q(s) = 1$, the stronger the error suppression ability. However, $Q(s)$ is introduced but brings noise PQ to the system from the noise transfer function (17), so it should make $Q(s) = 0$ as much as possible. On the one hand, the bandwidth of the Q-filter is required to be as high as possible to satisfy the antidisturbance performance in a wide-frequency range. On the other hand, the bandwidth of the Q-filter is limited by the system's robustness and noise. It can be seen that the balance of $|Q|$ and $|1 - Q|$ directly determines the antidisturbance and antinoise performance of the system. And they are hoped to be as small as possible simultaneously in the corresponding frequency domain.

For comparison with the conventional dual-rate loop structure, the closed-loop transfer function of the system without the addition of a DOB is derived here as follows:

$$\dot{\theta}_p = \frac{C_v MP}{1 + C_v MP}y_v + \frac{P}{1 + C_v MP}d + \frac{C_v MP}{1 + C_v MP}\zeta. \tag{18}$$

It shows that the addition of the observer does not change the transfer relationship between the input and output of the system if the modeling is accurate by comparison of (15) and (18). And it is found that a properly designed low-pass Q-filter can exert strong suppression on the dominant low-frequency disturbance input d when comparing (16) and (18). It is shown that the DOB structure cannot suppress the measurement noise of the external loop due to the physical characteristics of the sensor by comparing (17) and (18). However, on account of the flexible characteristic of the timing-belt system, it can isolate the disturbance created by these high-frequency signals. The flexible structure acts like an isolator that can naturally isolate the vibrations. These abovementioned comparisons demonstrate the superiority of applying the proposed DOB method to the flexible timing-belt system.

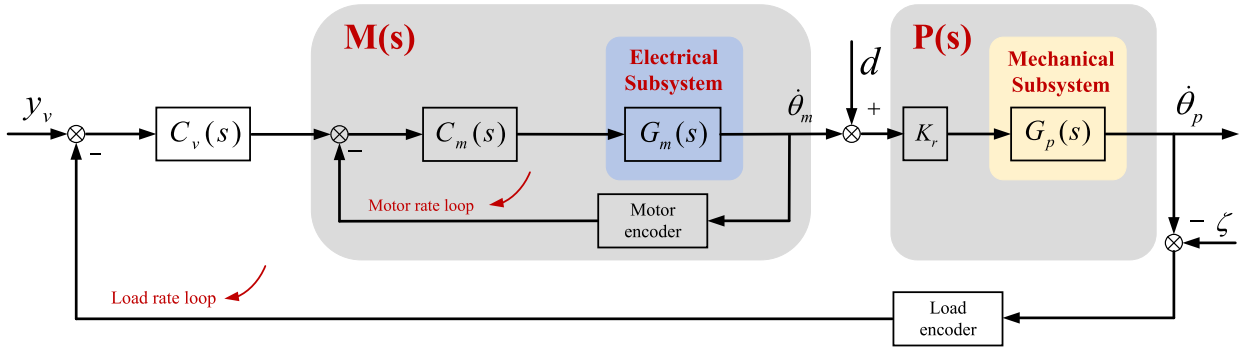

Fig. 4. Expression block diagram of the timing-belt-drive system.

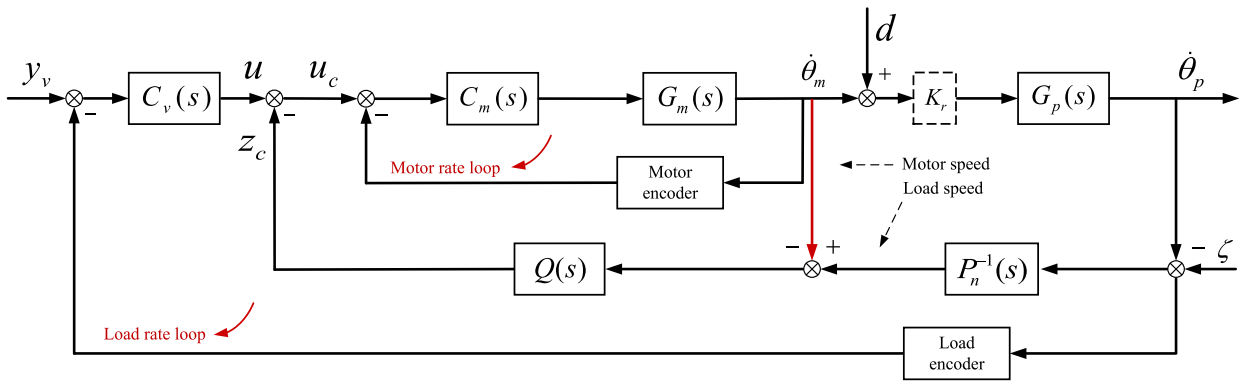

Fig. 5. DOB control based on the rate-difference information.

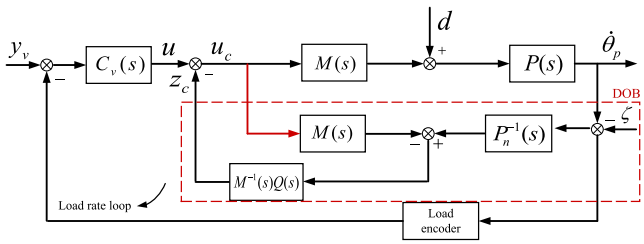

Fig. 6. Improved and simplified DOB control structure.

C. Stability Performance Analysis

The closed-loop transfer function of the speed control loop can be written as follows based on the abovementioned analyses:

$$\Phi(s) = \frac{C_v MP}{1 + C_v MP + (PP_n^{-1} - 1)Q}. \tag{19}$$

The characteristic polynomial is $D(s) = 1 + C_v MP + (PP_n^{-1} - 1)Q$. The system is stable if all the poles are in the unit circle. While it is not easy to get the pole distribution by solving $D(s)$. Now, making the equation transform into as follows:

$$D(s) = (1 + C_v MP)\left[1 + \frac{(PP_n^{-1} - 1)Q}{1 + C_v MP}\right]. \tag{20}$$

It shall be stable because the left term $1 + C_v MP$ is the original characteristics polynomial. According to the small-gain theorem, the stability condition of this control system should satisfy the following equation:

$$\left\| \frac{(PP_n^{-1} - 1)Q}{1 + C_v MP} \right\|_\infty < 1. \tag{21}$$

That is, the following constraints for the Q-filter should be met:

$$\|Q\|_\infty < \left\| \frac{1 + C_v MP}{PP_n^{-1} - 1} \right\|_\infty. \tag{22}$$

With the increase of frequency, the magnitude response of $1 + C_v MP$ gradually decreases from infinity to one. $PP_n^{-1} - 1 \approx 0$ is well-founded when $P(s) \approx P_n(s)$ is satisfied. It is thereby obvious that (22) is easy to reach if $Q(s)$ is designed to a lower bandwidth than the frequency in which $P(s)$ can be modeled accurately. When the error between the nominal model $P_n(s)$ and the real object $P(s)$ is defined as the multiplicative perturbation $\Delta(s)$, $P(s) = P_n(s)(1 + \Delta(s))$ is substituted into (20). Then, $\|\Delta(s) \cdot Q\|_\infty < 1$ should be satisfied. This means all points of the uncertain part $1/\Delta(s)$ must be larger than any point of the Q-filter on the magnitude–frequency curve. The system uncertainty $\Delta(s)$ will grow with the increase of the given frequency and the bandwidth of Q-filter will be compressed continuously.

D. Robust Performance Analysis

It can be known that the filter bandwidth is limited by the high-frequency noise of the system from the previous stability analysis, so that the control performance is compromised. This

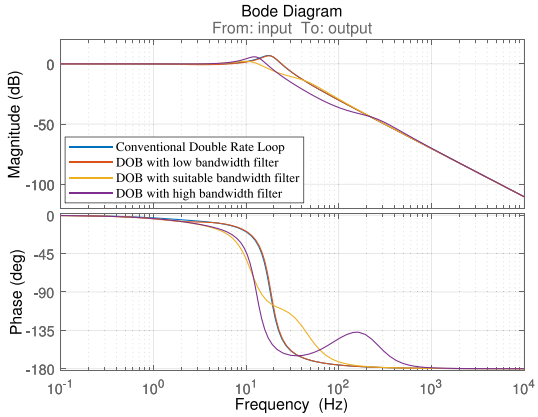

Fig. 7. Bode diagram of the closed-loop system.

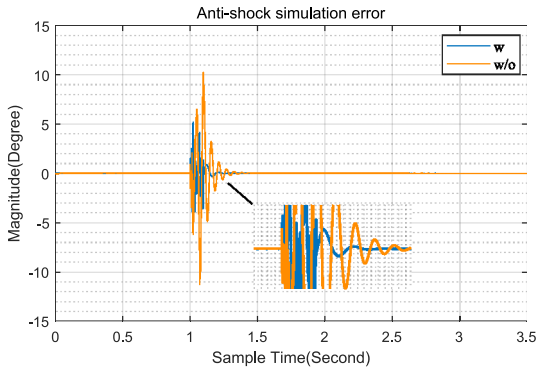

Fig. 8. Strong vibration experiment.

control structure needs to be tested under harsh conditions in order to verify the robustness of the system. And the closed-loop performance is analyzed, which is shown in Fig. 7, in the case of 20% uncertainty in low-frequency modeling and the impossibility of accurate modeling at 15 Hz. It is found that the higher the filter bandwidth, the higher the system stability margin. However, the stability margin starts to decrease and the stability of the system begins to be affected when the filter bandwidth exceeds a certain value. In general, the stability margin of the system is always higher than that without DOB under the condition of satisfying stability.

In addition, strong disturbance experiments are carried out to further verify the shock resistance of the system. In the case of 40% uncertainty in low-frequency modeling and the impossibility of accurate modeling at 5 Hz, a large disturbance is implemented to the system at 1 s, which is shown in Fig. 8. It can be seen that the error suppression is very effective under the condition of satisfying the system stability, especially in the region with severe backlash, where the error peak is significantly suppressed. An additional pair of conjugate poles and another pair of conjugate zeros are added to the system model $P(s)$ to better simulate the higher order modes in the real system. Under this stronger disturbance, as shown in Fig. 9, it can be seen that the overall disturbance suppression performance has begun to decline, and remains effective only on the suppression of commutation spikes.

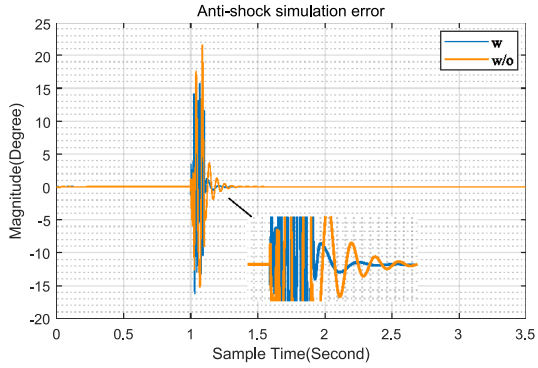

Fig. 9. Intense, strong vibration experiment.

E. Antidisturbance Performance Analysis

It is assumed that the disturbance suppression functions ($E(s) = e/d$) before and after adding the observer are E_1 and E_2, respectively. The following equation can be obtained:

$$\left|\frac{E_1}{E_2}\right| = \left|\frac{1-Q+PP_n^{-1}Q+C_vMP}{(1+C_vMP)(1-Q)}\right| = \left|\frac{1+\frac{PP_n^{-1}Q}{1-Q}+\frac{C_vMP}{1-Q}}{1+C_vMP}\right|. \tag{23}$$

The range of filter values is $0 < |Q| < 1$ because of the natural properties. There is $(C_vMP)/(1-Q) > C_vMP$ in the whole frequency domain, which proves that $|E_1/E_2| > 1$ is reasonable. It demonstrates that the disturbance suppression ability of the system is enhanced with the addition of the observer. Moreover, the change of system characteristics is considered during the transmitting motion, such as $P \to P'$. The transfer functions of system are expressed as follows:

$$W_1 = \frac{C_vMP}{1+C_vMP} \tag{24}$$

$$W_1' = \frac{C_vMP'}{1+C_vMP'} \tag{25}$$

$$W_2 = \frac{C_vMP}{1-Q+PP_n^{-1}Q+C_vMP} \tag{26}$$

$$W_2 = \frac{C_vMP'}{1-Q+P'P_n^{-1}Q+C_vMP'}. \tag{27}$$

Then, the sensitivity function of the system is defined as

$$S_{P'}^{W_1} = \left|\frac{\Delta W_1(s)/W_1(s)}{\Delta P(s)/P(s)}\right| = (1+C_vMP')^{-1} \tag{28}$$

$$S_{P'}^{W_2} = \left|\frac{\frac{\Delta W_2(s)}{W_2(s)}}{\frac{\Delta P(s)}{P(s)}}\right| = \left(1+\frac{P'P_n^{-1}Q}{1-Q}+\frac{C_vMP'}{1-Q}\right)^{-1} \tag{29}$$

$|S_{P'}^{W_2}| < |S_{P'}^{W_1}|$ can be proved in the frequency domain. This indicates that the DOB control structure is less sensitive to the parameter variations than the traditional dual-rate loop structure during transmitting motion. In other words, the DOB control system is capable and adaptable in face of those sudden and

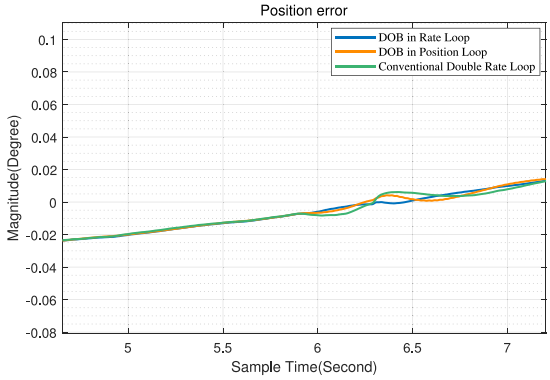

Fig. 10. Comparison experiments with conventional methods.

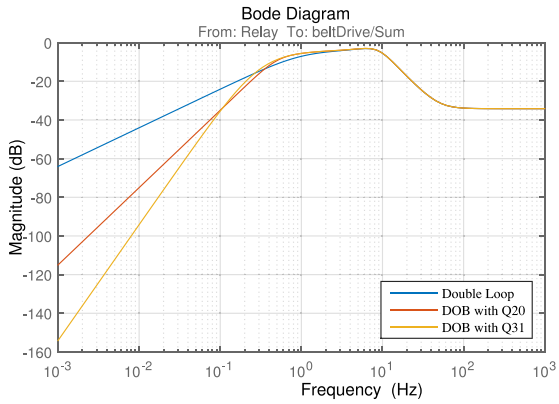

Fig. 11. Disturbance suppression curves with different filters.

strong parameter perturbations. The abovementioned sensitivity analysis is based on the DOB implementation in the rate loop. In addition, a comparative experiment of DOB implementation in the position loop is conducted in order to demonstrate the excellent performance of the proposed structure. Fig. 10 simulates the velocity commutation at 6–6.5 s, and it can be found that the scheme implemented in the rate loop proposed in this article does have faster response and better rejection than the conventional double rate loop or DOB implemented in the position loop. It confirms that the bandwidth of the rate loop is higher than that of the position loop, and its effect is significant.

F. Optimal Q-Filter Design

Several standard types of low-pass filters, such as Butterworth type and binomial coefficient type, are commonly used in the design of DOB. A common form of a low-pass filter is written as follows [30]:

$$Q(s) = \frac{1 + \sum_{k=1}^{N-r} a_k(\tau s)^k}{1 + \sum_{k=1}^{N} a_k(\tau s)^k} \tag{30}$$

where N is the highest exponential order of the denominator polynomial, r is the relative order, and τ is the time constant, which determines the filter bandwidth directly. The design of the filter must consider the regularization of $M^{-1}(s)Q(s)$ first. Since the relative order of M is $r = 2$, in the principle of simplicity, Q_{20} and Q_{31} filters are selected for the research. The disturbance suppression curves of the control system with different bandwidths of Q-filters are investigated as follows:

$$Q_{20}(s) = \frac{1}{(\tau s)^2 + 2(\tau s) + 1} \tag{31}$$

$$Q_{31}(s) = \frac{3(\tau s) + 1}{(\tau s)^3 + 3(\tau s)^2 + 3(\tau s) + 1}. \tag{32}$$

Compared with the dual-rate loop structure, the disturbance suppression ability of the DOB control system has been improved in the low-frequency domain, as shown in Fig. 11. The suppression effect of Q_{31} is better than that of Q_{20}. Equation (16) causes the amplification at the frequency of around 8 Hz, in which the waterbed effect also emerges. In the high-frequency domain, the consistent disturbance suppression performances of less than 0 dB are achieved for different bandwidths of filters due to the limit of active disturbance suppression ability of system.

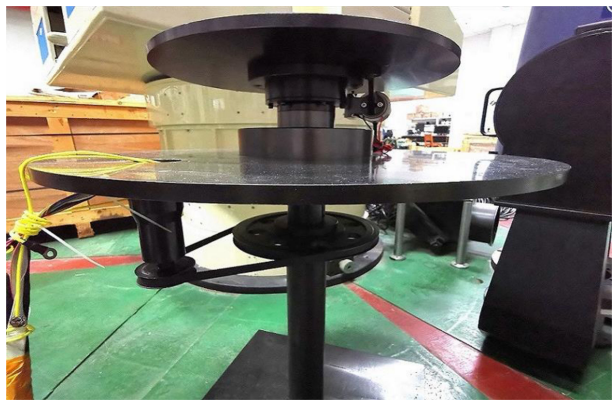

Fig. 12. Experimental system.

IV. Experimental Setup and Validation

A. System Layout

As it is shown in the following, a mechanical rotating platform driven by the timing-belt is presented. It consists of a brushless dc motor, gearbox reducer, photoelectric encoder, timing-belt, load, and control cabinet. The power of 40 W motor can provide the torque with a maximum speed of 9250 r/min and a nominal speed of 7220 r/min. The transmission ratio of gearbox is 132. The encoder accuracy of motor axis is 1000 lines fourth octave, and the load-side employs a 26-bit high-precision encoder. The sampling frequency of the control system is set as 1 kHz.

B. Parameters Design

Electrical subsystem and mechanical subsystem are modeled as second-order and first-order systems, respectively, in Section II. $M(s)$ and $P(s)$ are modeled as a second-order system in Section III. Under these assumptions, multiple open-loop frequency response tests are processed on the control object to obtain a reliable system model. Three frequency response curves at different turntable positions are shown in Fig. 13, and two conclusions can be drawn: 1) The rough assumption of system

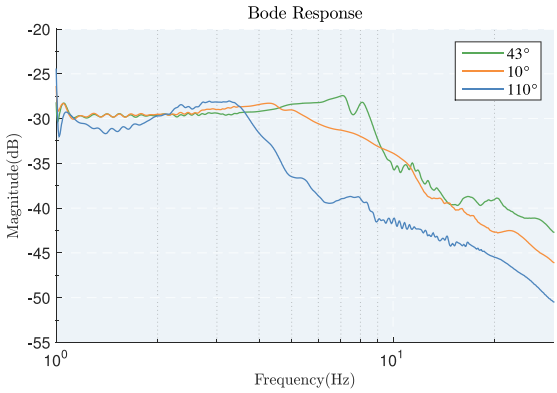

Fig. 13. Curves of frequency response tests.

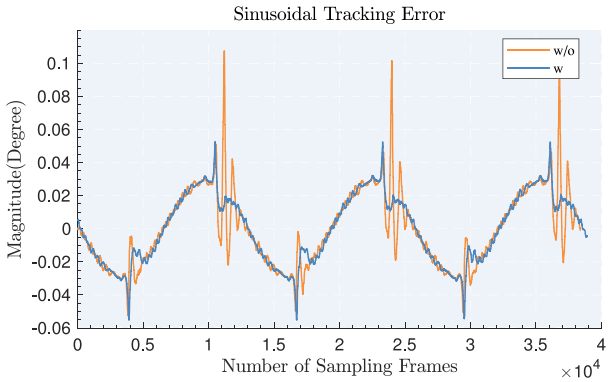

Fig. 14. Comparison of position errors of sinusoidal tracking.

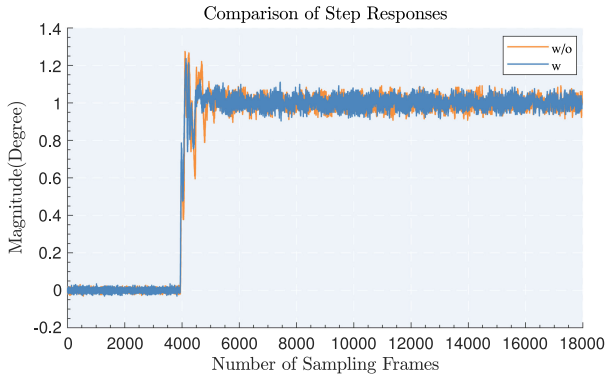

Fig. 15. Curves of step response tests.

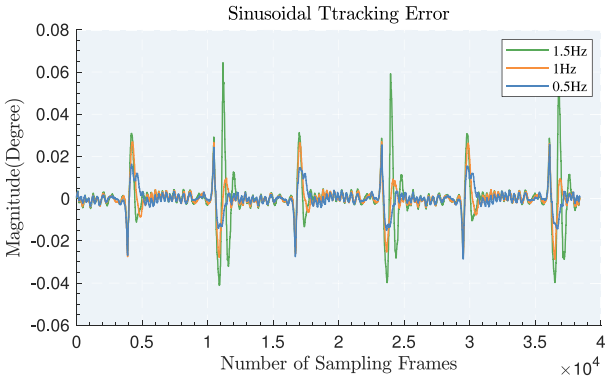

Fig. 16. Position errors with different filters.

bandwidth is around 7 Hz. 2) The overlap of frequency response curves above 1 Hz is not enough, indicating that the model above 1 Hz may be inaccurate.

Based on the first conclusion and assuming that the closed-loop of the motor driven by the commercial driver has a high bandwidth around 50 Hz, a rough model of $M(s)$ and $P(s)$ can be derived as follows:

$$M(s) = \frac{1}{1.013e-05\,s^2 + 0.004501s + 1} \tag{33}$$

$$P(s) = \frac{1.013e-05\,s^2 + 0.004501s + 1}{0.0005169\,s^2 + 0.03215s + 1}. \tag{34}$$

According to the second conclusion and (22), the system may achieve its optimal performance only by keeping the Q-filter within 1 Hz or a smaller cut-off bandwidth. Assuming that the cut-off bandwidth of the Q-filter is 0.5 Hz, the model of the Q-filter can be deduced as follows:

$$Q_{31}(s) = \frac{1.54s + 1}{0.1353\,s^3 + 0.7907\,s^2 + 1.54s + 1}. \tag{35}$$

C. Experimental Results

To perform the experiments of precise position of the turntable, a position controller is incorporated to form the three-loop control structure. The reference trajectory of the position loop is set as $\theta = 5\sin(0.5t)(^\circ)$. Due to the complex disturbance factors when the turntable speed is reversed, the obvious speed-commutation spikes and chatters can be seen on one-side when the observer is not equipped. Then, the spikes on this side are largely eliminated when the observer is added, which is shown in Fig. 14. The peak of position error decreases from 0.1° to 0.05°; the chatters of speed-commutation also have been eliminated slightly. The RMSE of position reduces from 0.0231 to 0.0207. This study makes some improvements to the existing research. For example, [31] shares similar conditions with our study but the method proposed in this article suppresses errors within 0.1 mrad and is easier to implement. A step response test is supplemented, as shown in Fig. 15, in order to test the transient response performance. It can be found that the proposed method responds faster than the traditional method, while eliminating certain spikes and chatters.

If continuing to add the reference signal feedforward to the speed control loop to predict the velocity in advance, a three-degree-of-freedom control structure consisting of feedforward, feedback, and observer will be formed. It will be more beneficial to reduce the response delay and average tracking error. A significant reduction of the error occurs beyond the speed-commutation region when adding the feedforward control. The RMSE of position continues to decline from 0.0207 to 0.0052. Furthermore, three cases are compared and all results are shown in Fig. 16 in order to find the optimal bandwidth of the Q_{31}-filter. The result shows that the 0.5 Hz filter of them is the most effective, which indicates the modeling is accurate enough below 0.5 Hz. Fig. 17(a) compared with the static position error

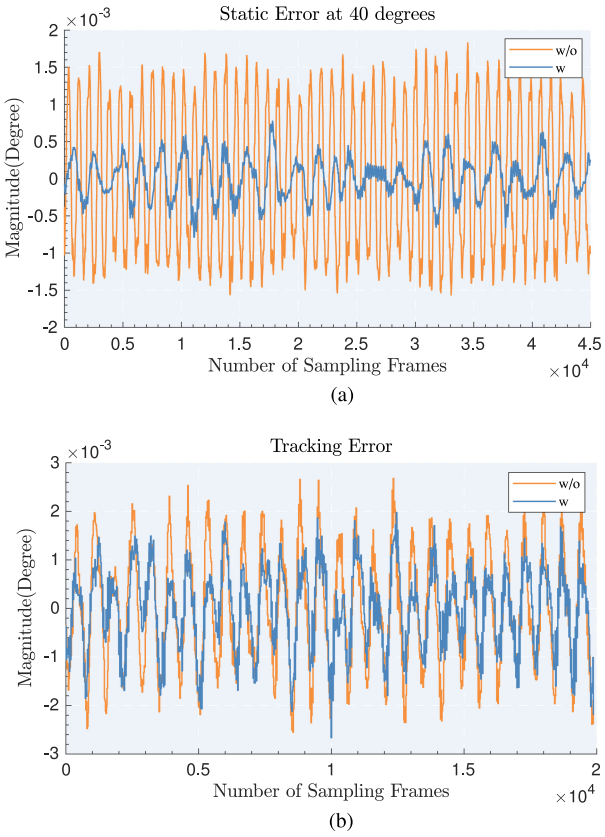

Fig. 17. Comparisons of tracking errors under different conditions. (a) Static tracking errors at the fixed-point of $\theta = 40°$. (b) Tracking errors at the linear speed of $\theta = 1.0t(°)$.

under the fixed-point experiment, there is an error attenuation of more than twice as much. Fig. 17(b) shows the straight-line tracking for $\theta = 1.0t(°)$. The linear tracking does not require the speed-commutation, and the improvement of suppression effect is not as obvious as the sinusoidal tracking. There is a 5–25% improvement in the low- and medium-speed region.

V. Conclusion

An improved DOB control structure was proposed in this article in order to suppress the uncertain disturbance in the transmission process of the flexible timing-belt-drive servo system. The modelings of the electrical and mechanical subsystems for this DOB in timing-belt servo system were first analyzed. Then the rate-difference signal between the load-side and the motor-side was applied to implement the DOB control structure. The rate information on the motor-side can be replaced with the input signal of inner loop due to a relative high bandwidth of inner motor loop, which avoids incorporating a rate sensor and also reduces the size and weight. The conditions for satisfying robust stability and the optimal structural settings of the Q-filter were analyzed. The proposed control structure was verified by the extensive experiments, and the parameters were adjusted to balance the antidisturbance and antinoise performances.

The application of the DOB control structure is not limited to the belt-drive control systems, the scheme can be extended to the antidisturbance research of other servo control systems. The modified DOB controller relies on a simple Q-filter and a low-frequency device model; therefore, the effective disturbance suppression can be easily achieved in limited control bandwidth. The next step in this research is to focus on the disturbance torque near the resonance frequency of the timing-belt due to elastic tension, which may require the elaboration of efficacious mathematical modeling. Efficient noise reduction methods are considered to improve the stability.

References

[1] G. Cepon and M. Boltezar, "Dynamics of a belt-drive system using a linear complementarity problem for the belt-pulley contact description," *J. Sound Vib.*, vol. 319, no. 3, pp. 1019–1035, 2009.

[2] Y. Zhang, G. Wang, B. Liu, W. Wang, and Y. Liu, "Fuzzy controller optimization of synchronous belt drive system based on improved whale optimization algorithm," in *Proc. 3rd Int. Conf. Robot. Automat. Sci.*, Jun. 2019, pp. 196–200.

[3] S. K. Kommuri, J. J. Rath, and K. C. Veluvolu, "Sliding-mode-based observer-controller structure for fault-resilient control in DC servomotors," *IEEE Trans. Ind. Electron.*, vol. 65, no. 1, pp. 918–929, Jan. 2018.

[4] S.-K. Tseng, T.-H. Liu, J.-W. Hsu, L. R. Ramelan, and E. Firmansyah, "Implementation of on-line maximum efficiency control for a dual-motor drive system," in *Proc. IECON- 40th Annu. Conf. IEEE Ind. Electron. Soc.*, 2014, pp. 655–660.

[5] F. da Fonseca Schneider, C. B. da Silva, P. J. Dias de Oliveira Evald, R. Sousa de Silva, and R. Z. Azzolin, "Backlash robotic systems compensation by inverse model-based PID control," in *Proc. IECON - 45th Annu. Conf. IEEE Ind. Electron. Soc.*, vol. 1, Oct. 2019, pp. 305–310.

[6] A. Anwar, X. Shao, Q. Hu, A. Moldabayeva, and B. Li, "Adaptive backstepping control of uncertain nonlinear systems with input backlash," in *Proc. IEEE Chin. Guid., Navigation Control Conf.*, Aug. 2016, pp. 1237–1242.

[7] A. G. Katsioula, Y. L. Karnavas, and Y. S. Boutalis, "An enhanced simulation model for DC motor belt drive conveyor system control," in *Proc. 7th Int. Conf. Modern Circuits Syst. Technol.*, 2018, pp. 1–4.

[8] A. Hace, K. Jezernik, and A. Sabanovic, "SMC with disturbance observer for a linear belt drive," *IEEE Trans. Ind. Electron.*, vol. 54, no. 6, pp. 3402–3412, Dec. 2007.

[9] N. Nevaranta, J. Parkkinen, T. Lindh, M. Niemela, O. Pyrhonen, and J. Pyrhonen, "Online estimation of linear tooth belt drive system parameters," *IEEE Trans. Ind. Electron.*, vol. 62, no. 11, pp. 7214–7223, Nov. 2015.

[10] P. Keadtipod, D. Banjerdpongchai, and P. Kittisupakorn, "Design of disturbance observer and model predictive control for non-minimum phase time-delay system with application to industrial boilers," in *Proc. 56th Annu. Conf. Soc. Instrum. Control Eng. Jpn.*, Sep. 2017, pp. 1389–1394.

[11] A. Sabanovic, O. Sozbilir, G. Goktug, and N. Sabanovic, "Sliding mode control of timing-belt servosystem," in *Proc. IEEE Int. Symp. Ind. Electron. (Cat. No.03TH8692)*, Jun. 2003, pp. 684–689.

[12] V. T. Minh, M. Tamre, and E. Sekhri, "Modeling and robust control algorithms for a linear belt driven system," *Open Comput. Sci.*, vol. 8, no. 1, pp. 142–153, 2018.

[13] M. Tanaka, Y. Pan, and K. Furuta, "Adaptive sliding mode control of belt driven prismatic manipulator," in *Proc. Int. Workshop Variable Struct. Syst.*, 2006, pp. 379–384.

[14] Y. Yildiz, A. Sabanovic, and K. Abidi, "Sliding-mode neuro-controller for uncertain systems," *IEEE Trans. Ind. Electron.*, vol. 54, no. 3, pp. 1676–1685, Jun. 2007.

[15] X. Ma, "Genetic taboo hybrid strategy for PID regulator parameter adaptation in belt conveyor," in *Proc. Int. Conf. Mach. Learn. Cybern.*, Aug. 2006, pp. 607–612.

[16] Z. Yang and L. Cai, "Tracking control of a belt-driven position table using Fourier series based learning control scheme," in *Proc. IEEE Int. Conf. Robot., Intell. Syst. Signal Process.*, 2003, pp. 196–201.

[17] Y. Liu, Z. Zhao, and W. He, "Stabilization of an axially moving accelerated/decelerated system via an adaptive boundary control," *ISA Trans.*, vol. 64, pp. 394–404, 2016.

[18] E. Sariyildiz, R. Oboe, and K. Ohnishi, "Disturbance observer-based robust control and its applications: 35th anniversary overview," *IEEE Trans. Ind. Electron.*, vol. 67, no. 3, pp. 2042–2053, Mar. 2020.

[19] D. K. Prasanga, E. Sariyildiz, and K. Ohnishi, "Compensation of backlash for geared drive systems and thrust wires used in teleoperation," *IEEJ J. Ind. Appl.*, vol. 4, pp. 514–525, Sep. 2015.
[20] M. Hong, W. Yao, Z. Zhu, and Y. Guo, "A hybrid PID controller for flexible joint manipulator based on state observer and singular perturbation approach," in *Proc. 39th Chin. Control Conf.*, Jul. 2020, pp. 3599–3603.
[21] J. Gui, L. Zhang, S. Li, and X. Wang, "Nonsingular terminal sliding mode control for PMSM servo system based on backlash compensation and high-order sliding mode observer," in *Proc. Chin. Control Decis. Conf.*, Aug. 2020, pp. 2873–2878.
[22] N. Kamaldin, S.-L. Chen, X. Li, C. S. Teo, and K. K. Tan, "A novel robust, continuous, PID-assisted control for precision tracking of flexible systems a case study on timing belts," in *Proc. IEEE Int. Conf. Adv. Intell. Mechatronics*, 2017, pp. 448–453.
[23] G. Zong, Y. LI, and H. Sun, "Composite anti-disturbance resilient control for Markovian jump nonlinear systems with general uncertain transition rate," *Sci. China: Inf. Sci. (English Ed.)*, vol. 62, no. 2, pp. 97–114, Jan. 2019.
[24] D. Yang, G. Zong, and H. R. Karimi, "H_∞ refined antidisturbance control of switched LPV systems with application to aero-engine," *IEEE Trans. Ind. Electron.*, vol. 67, no. 4, pp. 3180–3190, Apr. 2020.
[25] J. S. Bang, H. Shim, S. K. Park, and J. H. Seo, "Robust tracking and vibration suppression for a two-inertia system by combining backstepping approach with disturbance observer," *IEEE Trans. Ind. Electron.*, vol. 57, no. 9, pp. 3197–3206, Sep. 2010.
[26] G. Magnani, P. Rocco, L. Bascetta, and A. Rusconi, "On the use of torque disturbance observers in 2-mass systems with application to a robotic joint," in *Proc. IEEE Int. Conf. Mechatronics*, 2013, pp. 798–803.
[27] M. J. Kim and W. K. Chung, "Robust control of flexible joint robots based on motor-side dynamics reshaping using disturbance observer (DOB)," in *Proc. IEEE/RSJ Int. Conf. Intell. Robots Syst.*, 2014, pp. 2381–2388.
[28] T. V. Trung and M. Iwasaki, "Double-disturbance compensation design for full-closed cascade control of flexible robots," in *Proc. IEEE Int. Conf. Mechatronics*, 2021, pp. 1–6.
[29] T. Tang, S. Chen, X. Huang, T. Yang, and B. Qi, "Combining load and motor encoders to compensate nonlinear disturbances for high precision tracking control of gear-driven gimbal," *Sensors*, vol. 18, no. 3, Mar. 2018, Art. no. 754, doi: 10.3390/s18030754.
[30] A. Tesfaye, H. S. Lee, and M. Tomizuka, "A sensitivity optimization approach to design of a disturbance observer in digital motion control systems," *IEEE/ASME Trans. Mechatronics*, vol. 5, no. 1, pp. 32–38, Mar. 2000.
[31] K. H. Kim, J. K. Lee, B. S. Park, and S. K. Min, "Chatter-free sliding mode control for inertial stabilization of OTM (on-the-move) antenna driven by gear and flexible shaft," *Int. J. Precis. Eng. Manuf.*, vol. 13, no. 8, pp. 1317–1325, 2012.

Zhiyong Yu was born in Guizhou, China. He received the B.E. degree in measurement and control technology and instruments from the Department of Control, Shandong University of China, Jinan, China, in 2018. He is currently working toward the Ph.D. degree in measurement technology and instruments with the University of Chinese Academy of Sciences, Beijing, China.

His research interests include signal detection, optical precision tracking, and nonlinear control system design and measurement.

Tao Yang was born in Chongqing, China. He received the B.Sc. degree in electronic engineering from the University of Science and technology of China, Anhui, China, in 2008 and the M.S. degree in control engineering from the University of Chinese Academy of Sciences, Beijing, China, in 2014.

In 2008, he joined the Institute of Optics and Electronics, Chinese Academy of Sciences. His research interests include laser communication, control system design of gimbal, and fast steering mirror.

Yong Ruan was born in Chongqing, China. He received the B.E. degree from the Department of Automation, South-Central Minzu University, Wuhan, China, in 2017, and the M.S. degree in detection technology and automation device in 2020 from the University of Chinese Academy of Sciences, Beijing, China, where he is currently working toward the Ph.D. degree in signal and information processing.

His research interests include control-based sensors, servo control, inertial stabilization, and optical signal processing.

Tianrong Xu was born in Shandong, China. She received the B.E. degree in measurement and control technology and instruments from the Chongqing University of China, Chongqing, China and the M.S. degree in computer application technology from the University of Chinese Academy of Sciences, Beijing, China, in 2017 and 2020.

In 2020, she joined the Institute of Optics and Electronics, Chinese Academy of Sciences, where she is currently a Research Assistant. Her research focuses on the vibration rejections of tip-tilt mirror in moving platform.

Tao Tang (Member, IEEE) was born in Hubei, China. He received the Ph.D. degree in mechanical engineering from the University of Chinese Academy of Sciences, Beijing, China, in 2009.

From then on, he has joined the Institute of Optics and Electronics, Chinese Academy of Sciences, where he is currently a Full-Time Professor. From 2014 to 2016, he was with the Mechanical System Control Laboratory, University of California, Berkeley, Berkeley, CA, USA. His research interests include mechanical control system, including inertial stabilization technology, vibration rejections, and image-based visual servoing system.

Prof. Tang was the Recipient of the Youth Innovation Promotion Association, Chinese Academy of Sciences in 2013.